4-25-2019

Convergent evolution of hetero-oligomeric cellulose synthesis complexes in mosses and seed plants

Xingxing Li

Tori L. Speicher

Dianka CT Dees

Nasim Mansoori

John B. McManus

See next page for additional authors

Authors

Xingxing Li, Tori L. Speicher, Dianka CT Dees, Nasim Mansoori, John B. McManus, Ming Tien, Luisa M. Trindade, Ian S. Wallace, and Alison Roberts

Short title: Convergent evolution of cellulose synthesis complexes

Title: Convergent evolution of hetero-oligomeric cellulose synthesis complexes in mosses and seed plants

Xingxing Li[a], Tori L. Speicher[b], Dianka Dees[c], Nasim Mansoori[c], John B. McManus[d], Ming Tien[d], Luisa M. Trindade[c], Ian S. Wallace[b], Alison W. Roberts[a*]

[a]Department of Biological Sciences, University of Rhode Island, Kingston, Rhode Island 02881, USA

[b]Department of Biochemistry and Molecular Biology, University of Nevada, Reno, Nevada 89557, USA

[c]Wageningen UR Plant Breeding, Wageningen University and Research, Droevendaalsesteeg 1, 6708 PB Wageningen, the Netherlands

[d]Department of Biochemistry and Molecular Biology, The Pennsylvania State University, University Park, Pennsylvania 16802, USA

*Corresponding author: aroberts@uri.edu

Author contributions: A. W. R., I. S. W., and L. M. T conceived the project. A. W. R., I. S. W., L. M. T, and M. T. supervised experiments; X. L., T. L. S., D. D., and N. M. designed and performed experiments and analyzed the data; J. M. performed experiments; X. L., T. L. S., A. W. R., I. S. W., and L. M. T. wrote the manuscript.

Key word: cellulose, cellulose synthase, cellulose synthesis complex, cell wall, convergent evolution, *Physcomitrella patens*

Summary

In seed plants, cellulose is synthesized by rosette-shaped Cellulose Synthesis Complexes (CSCs) that are obligate hetero-oligomeric, comprising three non-interchangeable Cellulose Synthase (CESA) isoforms. The moss *Physcomitrella patens* has rosette CSCs and seven CESAs, but its common ancestor with seed plants had rosette CSCs and a single CESA gene. Thus, if *P. patens* CSCs are hetero-oligomeric, then CSCs of this type evolved convergently in mosses and seed plants. Previous gene knockout and promoter swap experiments showed that PpCESAs from class A (PpCESA3 and PpCESA8) and class B (PpCESA6 and PpCESA7) have non-redundant functions in secondary cell wall cellulose deposition in leaf midribs, whereas the two members of each class are redundant. Based on these observations, we proposed the hypothesis that the secondary class A and class B PpCESAs associate to form hetero-oligomeric CSCs. Here we show that transcription of secondary class A *PpCESA*s is reduced when secondary class B *PpCESA*s are knocked out and vice versa, as expected for genes encoding isoforms that occupy distinct positions within the same CSC. The class A and class B isoforms co-accumulate in developing gametophores and co-immunoprecipitate, suggesting that they interact to form a complex *in planta*. Finally, secondary PpCESAs interact with each other, whereas three of four fail to self interact when expressed in two different heterologous systems. These results are consistent with the hypothesis that obligate hetero-oligomeric CSCs evolved independently in mosses and seed plants and we propose the constructive neutral evolution hypothesis as a plausible explanation for convergent evolution of hetero-oligomeric CSCs.

Introduction

Cellulose is composed of (1,4)-β-linked glucan chains that associate laterally to form microfibrils, which are essential structural components of plant cell walls. Cellulose is synthesized by plasma membrane-localized cellulose synthesis complexes (CSCs) that exhibit a "rosette" structure in land plants and some green algae (Delmer, 1999, Somerville, 2006, McFarlane *et al.*, 2014). Within each CSC, Cellulose Synthase catalytic subunits (CESAs) catalyze the polymerization of individual glucan chains and are currently the only verified functional subunits (Kimura *et al.*, 1999, Guerriero *et al.*, 2010, McFarlane *et al.*, 2014, Purushotham *et al.*, 2016).

In Arabidopsis, primary and secondary cell wall cellulose is synthesized by different CSCs. Both types are hetero-oligomeric, containing three different non-interchangeable CESA isoforms that are required for CSC assembly and delivery to the plasma membrane. This functional specificity has been revealed through analysis of AtCESA mutant phenotypes, expression patterns, and protein-protein interactions (reviewed by Taylor, 2008, Endler and Persson, 2011, McFarlane *et al.*, 2014). *AtCESA4*, *AtCESA7*, and *AtCESA8* were first implicated in secondary cell wall cellulose deposition based on similar irregular xylem mutant phenotypes (Turner and Somerville, 1997, Taylor *et al.*, 1999, Taylor *et al.*, 2000, Turner *et al.*, 2001, Taylor *et al.*, 2003). These genes are co-expressed and non-redundant, with all three encoded proteins required for CSC assembly in xylem cells (Taylor *et al.*, 2000, Taylor *et al.*, 2003). Co-immunoprecipitation (Co-IP), membrane-based split ubiquitin yeast two-hybrid (MbYTH), and bimolecular fluorescence complementation (BiFC) experiments in *Nicotiana benthamiana* have demonstrated *in vivo* and *in vitro* interactions among AtCESA4, AtCESA7, and AtCESA8. (Taylor *et al.*, 2000, Taylor *et al.*, 2003, Timmers *et al.*, 2009). In contrast, *AtCESA1*, *AtCESA3*, and *AtCESA6*-like genes are implicated in primary cell wall cellulose deposition (Arioli *et al.*, 1998, Fagard *et al.*, 2000, Scheible *et al.*, 2001, Burn *et al.*, 2002, Robert *et al.*, 2004, Desprez *et al.*, 2007, Persson *et al.*, 2007). MbYTH, Co-IP, and BiFC experiments demonstrated *in vivo* and *in vitro* interaction among proteins encoded by these genes (Desprez *et al.*, 2007, Carroll *et al.*, 2012, Li *et al.*, 2013). Like the secondary cell wall *AtCESAs*, *AtCESA1* and *AtCESA3* are non-redundant, whereas *AtCESA6* is partially redundant with *AtCESA2* and *AtCESA5* (Desprez *et al.*, 2007, Persson *et al.*, 2007). Evidence that rosette CSCs contain 18 subunits (Nixon *et al.*, 2016, Jarvis,

2018) and that the CESA isoform stoichiometry is 1:1:1 for both primary and secondary cell wall CSCs in Arabidopsis (Gonneau *et al.*, 2014, Hill *et al.*, 2014) support a "hexamer of trimers" model in which three CESA isoforms occupy distinct positions within each lobe of their respective CSCs (Hill *et al.*, 2014, Nixon *et al.*, 2016, Jarvis, 2018). Phylogenetic analysis of CESA families has shown that all seed plants analyzed contain CESA sequences that cluster with members of each of the *Arabidopsis* primary and secondary CESA classes (Kumar *et al.*, 2009, Carroll and Specht, 2011, Jokipii-Lukkari *et al.*, 2017), indicating that hetero-oligomeric rosette CSCs with a hexamer of trimers organization evolved before the divergence of gymnosperms and angiosperms.

Rosette-type CSCs have also been observed by freeze-fracture electron microscopy in the model nonvascular plant *Physcomitrella patens* (Hedw.) Bruch & Schimp. (Roberts *et al.*, 2012, Nixon *et al.*, 2016). The *PpCESA* gene family includes seven members, but they form a cluster separate from the seed plant CESA classes (Roberts and Bushoven, 2007, Yin *et al.*, 2009, Carroll and Specht, 2011) indicating that moss and seed plant CESA families diversified independently from a single ancestral CESA that formed homo-oligomeric rosette CSCs (Roberts *et al.*, 2012). PpCESAs cluster in two moss-specific clades. Members of clade A, which comprises *PpCESA3*, *PpCESA5*, and *PpCESA8*, are not functionally interchangeable with the members of clade B, which comprises *PpCESA4*, *PpCESA6*, *PpCESA7*, and *PpCESA10*, indicating that clade A and clade B constitute two functional classes of PpCESAs (Scavuzzo-Duggan *et al.*, 2018).

Recently we showed that four PpCESAs, two members of class A (PpCESA3 or PpCESA8) and two members of class B (PpCESA6 or PpCESA7), participate in cellulose deposition in stereid cell secondary cell walls in *P. patens* leaf midribs (Norris *et al.*, 2017). Although single knockout (KO) mutants had little or no phenotype, both *ppcesa3/8*KO and *ppcesa6/7*KO lines had cellulose deficient midribs, suggesting that PpCESA3 and PpCESA8 from class A are redundant and that their role is distinct from that of PpCESA6 and PpCESA7, which constitute a second redundant pair from class B (Norris *et al.*, 2017). This was supported by promoter swap experiments showing that *ppcesa3/8*KO could be rescued by *PpCESA8pro:PpCESA3* or *PpCESA8pro:PpCESA8*, but not P*pCESA8pro:PpCESA7* (Norris *et al.*, 2017). These data are consistent with the hypothesis that CSCs responsible for secondary cell wall deposition in *P.*

patens are hetero-oligomeric with some positions that can be occupied by PpCESA3 or PpCESA8 (class A secondary PpCESAs) and others that can be occupied by PpCESA6 or PpCESA7 (class B secondary PpCESAs). If this hypothesis is correct, then hetero-oligomeric CSCs evolved independently in mosses and seed plants (Norris *et al.*, 2017). However, it has not been demonstrated that PpCESA3, PpCESA8, PpCESA6 and PpCESA7 reside in the same complex. In addition to *PpCESA* KO phenotype characterization (Norris *et al.*, 2017), gene expression analysis and protein-protein interaction assays can provide insight into CESA function and CSC composition in *P. patens*.

Here we report that expression of the class A secondary *PpCESA* genes is down-regulated when the class B secondary *PpCESA*s are knocked out and vice versa. In wild-type *P. patens*, accumulation of class A and B secondary PpCESA proteins is coordinated with gametophore development. We also show that both classes of proteins are pulled down together by Co-IP and that PpCESA3, PpCESA6, and PpCESA8 do not self-interact. These data support the hypothesis that PpCESA3, PpCESA8, PpCESA6 and PpCESA7 are members of obligate hetero-oligomeric CSCs responsible for secondary cell wall cellulose deposition in the stereid cells of *P. patens* gametophore leaf midribs and provide evidence for convergent evolution of hetero-oligomeric CSCs in mosses and seed plants.

Results

Transcript levels of secondary class A or class B *PpCESA*s are reduced when members of the other class are knocked out

In seed plants, the non-interchangeable CESA isoforms that form hetero-oligomeric CSCs are transcriptionally co-regulated (Brown *et al.*, 2005, Persson *et al.*, 2005). We showed previously that *PpCESA8* is up-regulated in *ppcesa3*KO lines, consistent with partial functional redundancy of these two members of class A (Norris *et al.*, 2017). However, we predicted that if class A and class B secondary PpCESAs occupy distinct sites within the same complex, then knocking out the genes that encode both class A members would result in down-regulation of the genes that encode the class B members and vice versa. To test this hypothesis we used RT-qPCR to analyze RNA extracted from leafy gametophores collected from *P. patens* wild type (three replicate cultures) and each of three independent lines of *ppcesa3*KO, *ppcesa8*KO,

*ppcesa3/8*KO, *ppcesa6/7*KO and *ppcesa4/10*KO. The results from two replicate experiments confirmed that *PpCESA3* and *PpCESA8* transcripts were significantly down-regulated in *ppcesa6/7*KO lines when compared to wild-type controls. Similarly, *PpCESA7* transcript levels were significantly down-regulated in *ppcesa3/8*KOs (**Figure 1, Figure S1**) and were not down-regulated in single *ppcesa3*KOs and *ppcesa8*KOs, as predicted if PpCESA7 can form a CSC with either PpCESA3 or PpCESA8. As reported previously, we were unable to design efficient primers that specifically amplify *PpCESA6* (Tran and Roberts, 2016), which is nearly identical to *PpCESA7* (Wise *et al.*, 2011). These genes exist as a tandem repeat in the *P. patens* genome and were knocked out as a pair (Norris *et al.*, 2017), so we were unable to test single *ppcesa6*KOs and *ppcesa7*KOs. Significant up-regulation of *PpCESA8* transcript in *ppcesa3*KO lines was detected in one experiment (**Figure 1, Figure S1**), consistent with previous results and partial redundancy of *PpCESA3* and *PpCESA8* as evidenced by the lack of a detectable mutant phenotype in *ppcesa3KO* (Norris *et al.*, 2017). The results for this treatment in the replicate experiment are not reported due to a technical problem affecting one sample. In our judgment it was unnecessary to conduct an additional replicate experiment given that up-regulation of *PpCESA8* in *ppcesa3*KO confirms previous results (Norris *et al.*, 2017). The lack of significant upregulation of *PpCESA3* transcript in *ppcesa8KO* (**Figure 1, Figure S1**) is consistent with previous results and the observation that*ppcesa8KO* has a weak mutant phenotype, unlike *ppcesa3KO* (Norris *et al.*, 2017).

In contrast to the secondary *PpCESA*s (*PpCESA3, PpCESA8,* and *PpCESA6/7*), expression of the other *PpCESA*s (*PpCESA4, PpCESA5* and *PpCESA10*) was not significantly different from wild type in any of the KO mutants with the exception of a small, but significant down-regulation of PpCESA4 in *ppcesa*6/7KO and significant up-regulation of *PpCESA5* in *ppcesa3/8* double KO (**Figure 1, Figure S1**). PpCESA4 has low overall expression in gametophores (Figure S1). PpCESA5 is in class A and is functionally interchangeable with PpCESA3 and PpCESA8 (Norris *et al.*, 2017). Because *ppcesa5*KOs produce no leafy gametophores (Goss *et al.*, 2012), the phenotype does not reveal whether PpCESA5 is necessary for secondary cell wall deposition and expression of the other *PpCESAs* in the *ppcesa5*KO gametophores could not be examined. Overall, these results indicate that *PpCESA3* and *PpCESA8* transcription is reduced in the absence of the mRNA or protein products of *PpCESA6* and *PpCESA7*, and that *PpCESA7* transcription is reduced in the absence of the mRNA or

protein products of *PpCESA3* and *PpCESA8*, as expected if CSC assembly requires at least one member of class A (PpCESA3 or PpCESA8) and one member of class B (PpCESA6 or PpCESA7).

<u>PpCESA3, PpCESA8 and PpCESA6/7 proteins co-accumulate at the onset of gametophore development</u>

To examine PpCESA protein abundance, polyclonal antibodies were generated to detect PpCESA3, PpCESA8, and PpCESA6/7, and specificity was assayed by western blot against microsomal protein fractions. For each antibody, a corresponding PpCESA overexpression line was used as a positive control, and the KO line was used as a negative control. Anti-PpCESA3 recognizes a band of the expected size (~120 kDa) in both *Act1pro:3xHA-PpCESA3* and wild-type **(Figure 2**A). This band was not detected in *ppcesa3*KO, indicating that Anti-PpCESA3 does not cross-reaction with other PpCESAs. We were unable to develop an antibody that distinguishes PpCESA6 and PpCESA7, which differ by only three amino acids (Wise *et al.*, 2011). Anti-PpCESA6/7, which was designed to recognize both isoforms, detected a 120 kDa band in *Act1pro:3xHA-PpCESA7* and wild-type, but not in *ppcesa6/7*KO (**Figure 2B**) indicating that it is specific to PpCESA6 and PpCESA7. Anti-PpCESA8 detected a 120 kDa band in *Act1pro::3xHA-PpCESA8* and Gd11. A weak 120 kDa band was detected in *ppcesa8*KO (**Figure 2C**). When *ppcesa3/8*KO was used as a negative control, no band was detected, suggesting that anti-PpCESA8 has weak cross-reactivity with PpCESA3 in addition to detecting PpCESA8, but does not cross-react with other PpCESAs.

Western blotting assays were used to examine the protein expression patterns for PpCESA3, PpCESA8, and PpCESA6/7 at different developmental stages. None of these proteins were detectable in 6-d-old wild-type Gd11 cultures consisting of pure protonema (**Figure 3)**. PpCESA3, PpCESA8, and PpCESA6/7 were all detected in 10-d-old cultures, which contained protonema, emerging gametophore buds, and young gametophores. Finally, larger amounts of these three PpCESAs were detected in 21-d-old cultures, which contained numerous leafy gametophores. These results indicate that PpCESA3, PpCESA8, and PpCESA6/7 exhibit similar protein expression profiles, with the highest abundance in the gametophores, consistent with

their role in gametophore development (Norris *et al.*, 2017) and the possibility that they function together within hetero-oligomeric CSCs.

PpCESA3, PpCESA8 and PpCESA6/7 co-precipitate

Although the rosette CSCs of *P. patens* are morphologically similar to the hetero-oligomeric seed plant CSCs, phylogenetic analysis indicates that their common ancestor had homo-oligomeric CSCs (Roberts *et al.*, 2012). Thus, hetero-oligomeric CSCs in *P. patens* would indicate an independent origin of this state. Based on the similarity of their mutant phenotypes (Norris *et al.*, 2017), protein accumulation profiles, and changes in their expression in specific *ppcesa*KOs, we hypothesized that PpCESA3, PpCESA6, PpCESA7, and PpCESA8 are present within the same hetero-oligomeric complexes. To test this hypothesis, we generated *P. patens* lines that expressed HA-tagged PpCESAs under the control of their native promoters in their cognate mutant backgrounds for use in Co-IP experiments. Complementation of the secondary cell wall cellulose deficiency was verified for both *PpCESA8pro*:*HA-PpCESA8* (*ppcesa8*KO background) and *PpCESA7pro*:*HA-PpCESA7* (*ppcesa6/7*KO background) lines. In both cases, the Potamine Fast Scarlet fluorescence of the midribs was restored (**Figure S2**). We could not verify complementation for *PpCESA3pro*::*HA-PpCESA3*, because we have not detected a phenotype for *ppcesa3*KO mutants (Norris *et al.*, 2017).

To analyze these Co-IP experiments, we first took a quantitative proteomics approach. Detergent solubilized membrane protein extracts prepared in triplicate from 15-d-old leafy gametophores of *PpCESA3pro*::*HA-PpCESA3* and wild type (negative control) were immunoprecipitated (IP) on magnetic anti-HA particles. Each set of eluted peptides was labeled with a unique TMT isobaric tag (TMT 126-128 for control samples, TMT 129-131 for HA-PpCESA3 IP samples, **Figure 4a**) and analyzed by mass spectrometry to determine the sample protein compositions and relative abundance ratios. Additionally, proteins that may interact to form a complex with PpCESA3 were postulated to be enriched in HA-PpCESA3 versus control samples (**Table 1**; **Figure 4b**).

Mass spectrometric analysis of IP samples from *PpCESA3pro*::*HA-PpCESA3* revealed that PpCESA3, PpCESA8, and PpCESA6/7 were enriched with average fold abundance changes

of 10.9, 7.8, and 6.2, respectively, compared to the control samples. These results suggest that PpCESA3 forms direct or indirect interactions with both PpCESA8 and PpCESA6/7 *in vivo* as expected if these isoforms are subunits of the same hetero-oligomeric complex. Ubiquitous membrane and photosynthetic proteins were also enriched with average abundance ratios >4. These proteins are mostly predicted to localize to chloroplasts or mitochondria, suggesting that they represent abundant sample contaminants that do not form meaningful interactions with PpCESA3 (**Table 1**). Overall, these results support the hypothesis that PpCESA3, PpCESA6/7, and PpCESA8 form hetero-oligomeric CSC.

Results from the quantitative mass spectrometry experiment were verified by western blotting. For the *PpCESA3pro*::*HA-PpCESA3* line (**Figure 5a**), blotting with anti-PpCESA3 showed that the IP antibody (anti-HA) successfully precipitated HA-PpCESA3 from the lysate of *PpCESA3pro*::*HA-PpCESA3*. When blotted with anti-PpCESA6/7 or anti-PpCESA8, the target proteins were found in the IP eluate indicating that PpCESA6 and/or PpCESA7 were co-precipitated with HA-PpCESA3, along with PpCESA8. In the Co-IP assay for *PpCESA8pro*::*HA-PpCESA8* (**Figure 5b**), blotting with anti-PpCESA8 verified that anti-HA pulled down the HA-PpCESA8. PpCESA6 and/or PpCESA7 and PpCESA3 were also detected in the IP eluate, indicating co-precipitation with the primary target. Similar results were observed when anti-HA was used to pull down HA-tagged PpCESA7 from the protein extracts of the *PpCESA7pro*::*HA-PpCESA7* transgenic line (**Figure 5c**). Again, HA-tagged PpCESA7 was precipitated, and PpCESA3 and PpCESA8 were co-precipitated. For the control experiment, Co-IP was carried out for wild-type *P. patens* (Gd11), which does not produce HA-tagged proteins (**Figure 5d**). None of the PpCESAs were immuno-detected showing that precipitation was dependent on the presence of the HA tag in one isoform. Taken together, these results are consistent with *in vivo* association of the secondary PpCESAs. We also tested all three IPs with anti-PpCESA5, which is specific for the PpCESA5 isoform (**Figure 2d**) that is required for development of the gametophore bud (Goss *et al.*, 2012). We did not detect PpCESA5 in either the total protein or eluate fractions of any of the IPs indicating that PpCESA5 is not abundant in gametophores and does not associate with the secondary PpCESAs *in vivo* (**Figure 5e**).

PpCESA3, PpCESA8 and PpCESA6 do not self-interact

Finally, we used two different assays to examine interactions between the PpCESA isoforms. Results from MbYTH assays show that PpCESA3, PpCESA8 and PpCESA6 do not strongly self-interact (**Figure 6**, **Table 2**). Although we observed some growth for the PpCESA3 self-interaction vs. no growth for the corresponding negative controls, the average was similar to other negative controls and only 20% of the corresponding positive control, consistent with very weak interaction. Strong positive interactions included PpCESA8 (bait) with PpCESA3 and PpCESA7, PpCESA6 (bait) with PpCESA8 and PpCESA7, and PpCESA7 (bait) with itself, PpCESA3 and PpCESA6. Weak interactions occurred between PpCESA3 (bait) and PpCESA7 and PpCESA8 (bait) and PpCESA6. Results of reciprocal tests with bait and prey switched were generally consistent. For two pairs, interactions were weak in one case and positive in the other case (PpCESA3 with PpCESA7 and PpCESA6 with PpCESA8). However, interactions of PpCESA8 with PpCESA3 and PpCESA7 yielded opposite results when PpCESA8 was the bait (positive) vs. the prey (negative).

Interactions were also tested using a BiFC assay in *N. benthamiana* (**Figure 7**, **Table 2**). For most interactions, the results confirmed the MbYTH results. PpCESA3 self-interaction was weak with MbYTH and negative with BiFC and the interaction between PpCESA3 and PpCESA7 was weak for MbYTH and strongly positive for BiFC. As in the MbYTH assay, reciprocal tests of the interactions of PpCESA8 with PpCESA3 and with PpCESA7 produced different results. The absence of detectable fluorescence in leaves expressing N-YFP-PIP2-1 + C-YFP-PpCESA7 (negative control), as well as six different N-YFP-PpCESA + C-YFP-PpCESA pairs that also failed to interact in the MbYTH assay, provides a control for YFP auto reconstitution (Horstman *et al.*, 2014). YFP fluorescence that was sometimes observed in nuclei may have arisen from soluble YFP detached from PpCESAs. It has been well documented that detached N-YFP and C-YFP cannot assemble and become fluorescent on their own, whereas pre-assembled N-YFP/C-YPF is stable and retains fluorescence when detached from interacting proteins (Ghosh *et al.*, 2000, Magliery *et al.*, 2005). Therefore, soluble YFP in the nucleus most likely arose from detachment of assembled N-YFP/C-YFP from interacting CESAs.

In summary, only class B-class B and class A-class B interactions were both strong and robust using different methods. Overall the results of protein interaction assays are consistent

with formation of hetero-oligomeric CSCs through interactions between distinct subunits and the inability of PpCESA3, PpCESA8 and PpCESA6 to form stable homo-oligomeric CSCs.

Discussion

Our previous genetic analyses showed that *ppcesa3/8*KOs and *ppcesa6/7*KOs have similar phenotypes characterized by severe reduction of cellulose deposition in the midribs of the gametophore leaves. Based on the non-redundancy of PpCESA3/8 with PpCESA6/7 in these experiments and the ability to complement *ppcesa3/8*KO with *PpCESA8pro:PpCESA3* or *PpCESA8pro:PpCESA8*, but not P*pCESA8pro:PpCESA7*, we proposed the hypothesis that the CSCs that synthesize the midrib secondary cell wall in *P. patens* are obligate hetero-oligomers requiring at least one isoform from class A (PpCESA3 or PpCESA8) and one isoform from class B (PpCESA6 or PpCESA7) (Norris *et al.*, 2017). Here, this hypothesis is further supported by 1) transcriptional down-regulation of secondary *PpCESA*s when members of the other class are knocked out (**Figure 1**), 2) coordinated accumulation of PpCESA3, PpCESA8, and PpCESA6/7 proteins in leafy gametophores (**Figure 3**), 3) co-IP of PpCESA3, PpCESA8, and PpCESA6/7 (**Figures 4 and 5**), and 4) the inability of PpCESA3, PpCESA8 and PpCESA6 to self interact (**Figures 6 and 7, Table 2**).

In *Arabidopsis*, the genes encoding CESA isoforms that function within the same CSCs are co-expressed (Fagard *et al.*, 2000, Taylor *et al.*, 2000, Scheible *et al.*, 2001, Hamann *et al.*, 2004, Brown *et al.*, 2005, Persson *et al.*, 2005, Betancur *et al.*, 2011, Li *et al.*, 2013). *AtCESA* overexpression enhances the expression of *AtCESA*s that encode members of the same CSC (Hu *et al.*, 2018) and accumulation of specific AtCESA proteins is diminished when another member of the CSC is absent (Desprez *et al.*, 2007, Hill *et al.*, 2014). We showed previously that *PpCESA3*, *PpCESA8*, *PpCESA6*, and *PpCESA7* have similar expression patterns, including in leaf midribs (Tran and Roberts, 2016). Consistent with redundant function as suggested by mutant phenotypes, *PpCESA8* is up-regulated when *PpCESA3* is knocked out (Norris *et al.*, 2017). However, when we comprehensively examined PpCESA expression in *ppcesa* mutants, we found that *PpCESA3* and *PpCESA8* are both down-regulated in *ppcesa6/7*KOs, and that expression of PpCESA6/7 is down-regulated in *ppcesa3/8*KOs (**Figure 1**). Thus, transcription of

11

each member of each class of secondary *PpCESA*s is responsive to the presence of the mRNA or protein products of members of the other class, as expected if they occupy distinct sites in the same CSC.

PpCESA3, PpCESA8 and PpCESA6/7 proteins were not detected in young cultures containing only protonema, but accumulated in older cultures containing gametophores (**Figure 3**). These observations are consistent with the cognate mutant phenotypes, which impair cellulose deposition in the midribs of gametophore leaves (Norris *et al.*, 2017). Similar protein co-expression patterns were observed in Arabidopsis where CESA proteins responsible for secondary cell wall deposition (AtCESA4, AtCESA7 and AtCESA8) were coordinately detected in developing vascular tissue (Turner *et al.*, 2001, Taylor *et al.*, 2003) and CESA proteins responsible for primary cell wall deposition (AtCESA3 and AtCESA6) were co-localized in elongating hypocotyls (Desprez *et al.*, 2007).

Co-IP of AtCESA4, AtCESA7 and AtCESA8 (Taylor *et al.*, 2003) and AtCESA3 and AtCESA6 (Desprez *et al.*, 2007) provided evidence to suggest that these proteins interact to form CSCs involved in secondary cell wall deposition (Taylor *et al.*, 2000, Taylor *et al.*, 2003, Atanassov *et al.*, 2009) and primary cell wall deposition (Desprez *et al.*, 2007) respectively. Using a similar approach, two types of CSCs (one containing PdxtCESA7A and PdxtCESA8B and the other one containing PdxtCESA1A and PdxtCESA3) were identified in the xylem of *P. trichocarpa* (Song *et al.*, 2010). In *P. patens*, PpCESA3, PpCESA8 and PpCESA6/7 were pulled down together when any one isomer was immunoprecipitated, as shown by western blotting (**Figure 5a-c**). Analysis by quantitative mass spectrometry also showed that PpCESA3 and PpCESA6/7 formed a stable complex with PpCESA8 *in vivo* (**Figure 4**). Although a few plasma membrane proteins were enriched along with the PpCESAs, the proteomic analysis is not consistent with mass non-specific precipitation of membrane proteins. We have also shown that the PpCESAs are pulled down only when one of them carries the HA tag (**Figure 5d**). In contrast to the secondary PpCESAs, PpCESA5 functions in primary cell wall deposition in gametophore buds and meristems (Goss *et al.*, 2012). Notably, PpCESA5 does not co-precipitate with the secondary PpCESAs (**Figure 5e**), indicating that the secondary PpCESAs form separate complexes.

Co-precipitation of PpCESA3, PpCESA8, and PpCESA6/7 does not rule out the possibility that the individual isomers can form homo-oligomeric complexes. However, the results of BiFC and MbYTH experiments indicate that PpCESA3, PpCESA8 and PpCESA6 do not self-interact strongly (**Figures 6, 7**). Each interaction was tested in four independent experiments, i.e. two different assays, each with reciprocal tagging or in replicate tests in the case of self-interactions. The MbYTH assay detects dimerization of membrane proteins expressed in yeast (Fetchko and Stagljar, 2004). Results from previous MbYTH studies with AtCESAs have not been fully consistent (Timmers *et al.*, 2009, Carroll *et al.*, 2012, Li *et al.*, 2013), highlighting the importance of corroborating these finding with other methods. The BiFC assay (Hu *et al.*, 2002, Walter *et al.*, 2004) detects interactions within plant membranes and has also been used to test interactions among AtCESAs (Desprez *et al.*, 2007, Timmers *et al.*, 2009, Carroll *et al.*, 2012). Although results from these types of assays must always be interpreted with caution, detection of weak or no self-interaction in four independent experiments (i.e. BiFC and MbYTH assays, replicate tests) indicates that PpCESA3, PpCESA8 and PpCESA6 are unlikely to form homo-oligomeric complexes in *P. patens*. Whereas PpCESA7 showed self-interaction in these assays, the cellulose deficient midrib phenotype of *ppcesa3/8* double knockout mutants, which is not rescued by expressing PpCESA7 under control of the *PpCESA8* promoter (Norris *et al.*, 2017), indicates that homo-oligomeric complexes composed of PpCESA7 alone are not sufficient for normal secondary cell wall deposition.

Our previous results suggested that convergent CESA sub-functionalization in the moss and seed plant lineages resulted from similar selective pressure favoring regulatory uncoupling of the CESAs that synthesize primary and secondary cell walls (Norris *et al.*, 2017). Taken together, evidence that the secondary PpCESAs form hetero-oligomeric CSCs (**Figures 4-7**), that class A and class B secondary PpCESAs are not interchangeable (Norris *et al.*, 2017, Scavuzzo-Duggan *et al.*, 2018), and that *PpCESA3*/*PpCESA8* and *PpCESA6*/*PpCESA7* constitute redundant pairs (Wise *et al.*, 2011, Norris *et al.*, 2017) is consistent with PpCESA neo-functionalization such that members of class A (PpCESA3 or PpCESA8) and class B (PpCESA6 or PpCESA7) occupy distinct positions within the CSCs (**Figure 8**). If PpCESA7 is unique in its ability to self-interact as indicated by results of MbYTH and BiFC results (**Figures 6,7**), then the

class B PpCESA may occupy two positions within each lobe (gray subunits in **Figure 8**). The lack of self interaction for the other secondary *P. patens* CESAs argues against a model in which hetero-oligomeric CSC are composed of distinct homo-trimeric lobes (Turner and Kumar, 2018). Experiments with Arabidopsis knockout mutants showed that the two remaining secondary AtCESA isoforms do not co-IP in the absence of the third isoform (Taylor *et al.*, 2003) and provided additional evidence for hetero-oligomeric CSC composed of three non-interchangeable CESA isoforms. However, because the *P. patens* secondary CSCs contain just two non-interchangeable isoforms, it is not possible to replicate these Arabidopsis experiments in *P. patens*.

Convergent CESA neo-functionalization in the moss and seed plant lineages can be explained by the constructive neutral evolution hypothesis (Haigler and Roberts, 2018), which posits that duplication of genes that encode members of homo-oligomeric complexes is followed by accumulation of neutral mutations that eventually alter protein-protein interfaces such that only non-identical subunits can interact. The genes encoding both subunits are subsequently maintained by selection, since neither subunit is capable of forming a functional homo-oligomeric complex (Doolittle, 2012, Finnigan *et al.*, 2012). This process functions as an evolutionary ratchet, driving neofunctionalization through modification of interfaces that existed in the original homo-oligomeric complex without changes in protein biochemical output (Doolittle, 2012, Finnigan *et al.*, 2012).

Emerging results indicate that the locations of the interfaces that determine class-specific interaction vary among CESA classes in Arabidopsis (Carroll and Specht, 2011, Kumar *et al.*, 2016, Hill *et al.*, 2018) and *P. patens* (Scavuzzo-Duggan *et al.*, 2018), as expected if hetero-oligomeric complexes evolved convergently. With only two functionally distinct CESA classes and more functional redundancy (Li, 2017, Norris *et al.*, 2017, Scavuzzo-Duggan *et al.*, 2018), it appears that CESA functional differentiation is less well developed in *P. patens* compared to seed plants. This likely reflects the relatively recent occurrence of genome duplications in *P. patens* (27-48 mya) (Lang *et al.*, 2018), whereas the duplications that generated the six seed plant CESA clades occurred before the divergence of gymnosperms and angiosperms, over 200 mya (Zeng *et al.*, 2014). Thus, the class-specific CESA-CESA interfaces in seed plants and mosses

may preserve, respectively, the results of ancient and more recent evolutionary experiments that can be exploited to reveal protein-protein interactions that underlie the assembly and stabilization of rosette CSCs. In this light, it is notable that we detected self-interaction for PpCESA7, but not PpCESA6, which differs from PpCESA7 by only three amino acids, L8V, G24S, and E26G (Wise *et al.*, 2011). All three substitutions are in the N-terminus, which is a highly disordered region (Scavuzzo-Duggan *et al.*, 2018) and not included in the currently available CESA structural model (Sethaphong *et al.*, 2013). Thus, an informed analysis of the functional significance of these mutations must await the results of ongoing efforts to refine CESA models.

Experimental Procedures

<u>Culture conditions</u>

Wild-type and transgenic *P. patens* lines were maintained on BCDAT plates and propagated by subculturing as previously described (Roberts *et al.*, 2011). To produce colonies with leafy gametophores, explants of 7-day-old protonemal tissue were transferred to BCD plates and cultured for 15 days. Gametophores were harvested with microdissection scissors for protein extraction.

<u>Vector construction</u>

Construction of the *PpCESA3pro::HA-PpCESA3* and *PpCESA8pro::HA-PpCESA8* expression vectors and *HA-PpCESA7* entry clone was described previously (Norris *et al.*, 2017). To construct the *PpCESA7pro::HA-PpCESA7* expression vector, entry clones containing the *PpCESA7* native promoter (Tran and Roberts, 2016) and the *HA-PpCESA7* entry clone were inserted into the Si3-pTH-GW destination vector (Tran and Roberts, 2016) using LR Clonase II Plus (Invitrogen, Grand Island, NY, USA) as described previously (Norris *et al.*, 2017). *PpCESA3pro::HA-PpCESA3* and *PpCESA7pro::HA-PpCESA7* were linearized with SwaI and *PpCESA8pro::HA-PpCESA8* was linearized with PciI for transformation into *P. patens*.

For MbYTH vectors, cDNA templates for *PpCESA7* (DQ160224) and *PpCESA8* (DQ902549) were obtained from RIKEN BioResource Center, Tsukuba, Ibaraki JP (clones pdp38142 and pdp39044, respectively). Preparation of cDNA templates for *PpCESA3* (PNR49373.1) and

PpCESA6 (DQ160224) was described previously (Scavuzzo-Duggan *et al.*, 2018). Bait vectors (Cub) were constructed by amplifying the full-length *PpCESAs* from cDNA templates as described previously (Timmers *et al.*, 2009) using Phusion DNA polymerase (Thermo Fisher Scientific, Waltham, MA, USA) and appropriate primers (Table S1) and ligating them into pTFB1 (Dualsystems Biotech AG, Zurich, Switzerland) in-frame and downstream of the C-terminal half of ubiquitin and the chimeric transcriptional reporter LexA-VP-16. Prey vectors (NubG) were constructed by ligating the amplified *PpCESAs* into pADSL-Nx (Dualsystems Biotech AG) in-frame and downstream of the N-terminal half of ubiquitin. All vectors were sequence verified.

For BiFC vectors, the full-length *PpCESA*s were amplified from cDNA templates as described previously (Timmers *et al.*, 2009) using appropriate primers (Table S1). The coding sequences were cloned into the Gateway-compatible destination vectors pBIFc-2 and pBIFc-3 in front of the constitutive 35S promoter (Hu *et al.*, 2002). The N-terminal and the C-terminal fragments of Yellow Fluorescent Protein (YFP) were both fused to the N-terminus of the coding sequences of the CESAs. All vectors were sequence verified.

Preparation of *P. patens* lines expressing hemagglutinin (HA)-tagged CESAs

PpCESA overexpression lines were used as positive controls for assaying antibody specificity, and were selected from transformations of *ppcesa5*KO-2 with vectors driving expression of 3X-HA-tagged PpCESA3, PpCESA5, PpCESA7 or PpCESA8 under control of the rice *Actin1* promoter (Scavuzzo-Duggan *et al.*, 2018).

Transgenic lines expressing HA-PpCESA3, HA-PpCESA8, and HA-PpCESA7 in the cognate KO lines were created for Co-IP with anti-HA. Protoplasts were prepared from lines *cesa8*KO-5B-lox (Tran *et al.*, 2018), and *cesa3*KO-5T (Norris *et al.*, 2017). The *hph* selection cassette was removed from *cesa6/7*KO-7A (Norris *et al.*, 2017) by Cre-mediated recombination of flanking *lox-p* sites (Vidali *et al.*, 2010) to allow transformation with *PpCESA7pro*::*HA-PpCESA7*, which confers hygromycin resistance. Protoplasts were prepared from a hygromycin sensitive line (*cesa6/7*KO-7A-lox) lacking the *hph* cassette. Protoplasts were transformed with the cognate *PpCESApro*::*HA-PpCESA* vector and stable transformants were selected with 15 μg

mL^{-1} hygromycin (Roberts *et al.*, 2011). Rescue of mutant phenotypes was tested for *cesa8*KO-5B-lox and *cesa6/7*KO-7A-lox as described previously (Norris *et al.*, 2017).

RNA extraction and Real-time quantitative PCR (RT-qPCR)

Wild type GD11 and three independent lines each of five different knockout genotypes described previously (Norris *et al.*, 2017) were tested for *PpCESA* expression. These lines included *ppcesa3*KO (5, 35, 126), *ppcesa8*KO (5B, 4C, 10C), *ppcesa3/8*KO (43, 57, 86), *ppcesa4/10*KO (1A, 4, 7), and *ppcesa6/7*KO (6A, 7A, 1D). Total RNA was extracted from gametophores harvested from 21-day old cultures and converted to cDNA as described previously (Tran and Roberts, 2016). RT-qPCR analysis (2 PCR replicates per sample) was performed using a Lightcycler 480 and SYBR Green I Master Mix (Roche, Basel, Switzerland) to monitor synthesis of double stranded DNA. The specificity and efficiency of primers used for RT-qPCR were verified previously (Tran and Roberts, 2016). Stable expression of reference genes *Actin* (*PpACT*) and *v-Type h+ Translocating Pyrophosphatase* (*PpVHP*) was demonstrated previously (Le Bail *et al.*, 2013). For relative quantification, PCR replicates were averaged, $2^{-\Delta Ct}$ values were calculated for each sample, and $2^{-\Delta\Delta Ct}$ values were calculated (Livak and Schmittgen, 2001) to determine fold-changes for each knockout genotype (three independent lines) relative to wild type (three independent RNA isolations). Each experiment was repeated using independently isolated RNA. Statistical analysis was performed on $2^{-\Delta Ct}$ values combined from replicate experiments (n=6) using the non-parametric Kruskal Wallis Test (vassarstats.net/kw4.html) to compare two or more knockout genotypes to the wild type. Alternatively, the non-parametric Mann Whitney Test for unpaired data (http://astatsa.com/WilcoxonTest/) was used in cases where only a single mutant genotype produced a signal because the other genotypes lacked the gene being measured.

Generation of polyclonal anti-PpCESAs

Peptide antigens were designed to regions of each PpCESA for the purpose of raising antibodies specific for each isoform (**Table S2**). A single peptide was designed for raising an antibody to recognize both PpCESA6 and PpCESA7, which differ by only 3 amino acids (Wise *et al.*, 2011). The peptides were synthesized chemically, conjugated to keyhole limpet

hemocyanin, and injected into New Zealand white rabbits (Covance Inc., Princeton NJ USA). For purification, the peptides were conjugated via the cysteine residue to Sulfolink Immobilization resin (Thermo Fisher Scientific) according to the manufacturer's instructions. The purification of PpCESA antibodies from total serum was carried out by affinity chromatography. Briefly, 10 mL of serum, buffered with WB (20 mM NaHPO$_4$, pH7.2, 50 mM NaCl) was incubated with the resin-linked peptides for 18h at 4°C. The resin was loaded onto a column and the flow through was passed over the resin twice. The resin was washed with 20 mL of WB followed by 10 mL of WB containing an additional 250 mM NaCl. Antibodies were eluted from the resin using 5 mL of EB (100 mM glycine, pH 2.5). Fractions of 250 μL containing NB (50 μL 1 M Tris-Cl, pH 8.0) were collected and mixed immediately to neutralize pH. Fractions containing PpCESA antibodies were identified by absorbance at 280 nm and combined. Glycerol was added to 30% and CESA antibodies were stored at -80°C. The specificity of each antibody was tested by western blotting against *P. patens* protein extracts.

Protein expression profiling of the PpCESAs

Wild type *P. patens* was cultured on solid BCD medium and a portion of the protonema was harvested on day 6 for protein extraction. On the seventh day remaining protonema was transferred to fresh solid BCD medium. Portions of this tissue were harvested on day 10 and on day 21 for protein extraction. Microsomal protein isolation and western blot analysis was processed as previously described (Scavuzzo-Duggan *et al.*, 2015). The primary antibody dilutions for anti-PpCESA3, anti-PpCESA5, anti-PpCESA6/7, and anti-PpCESA8 were 1: 8000, 1:5000, 1:1000, and 1: 50,000 respectively.

Co-immunoprecipitation

Co-immunoprecipitation (Co-IP) experiments were performed according to the methods from previous studies with some modifications (Desprez *et al.*, 2007, Song *et al.*, 2010). Tissue explants grown for 15 d and comprised mostly of leafy gametophores were compressed between layers of tissue to remove excess water and ground in liquid nitrogen, and the powder was combined with1 mL of ice-cold IP buffer [20mM Tris.HCl, pH7.5; 150mM NaCl; 5mM MgCl$_2$; 10% sucrose; 1% glycerol; 1mM EDTA; 1.5% CHAPS (Sigma, St. Louis, MO, USA); 1% protease inhibitor cocktail (Sigma, P9599); 1% phosphatase inhibitor mixture 2 (Sigma, P5726),

and 3 (Sigma, P0044); and 1% polyvinylpyrrolidone]. The tube was incubated on ice for 30 min with occasional inversion and centrifuged at 20,000 x g for 30 min to pellet insoluble debris. The supernatant was transferred to a new tube with 25 µL of Pierce Anti-HA Magnetic Beads (Thermo Fisher Scientific) and rotated (8 RPM) for 50 min on an end-over-end rotator (Thermo Fisher Scientific). Beads were then collected with a magnetic stand (Thermo Fisher Scientific), and the unbound sample was removed. 400 µL of TBS-T buffer (Scavuzzo-Duggan *et al.*, 2015) was added to the tube and gently mixed. Beads were collected again by magnetic stand, and the supernatant was discarded. This step was repeated twice. For the last wash, 400 µL of ultrapure water was added to the tube and gently mixed. Beads were collected on a magnetic stand, and the supernatant was removed. For elution, 50 µL of 2X SDS-PAGE sample buffer (Scavuzzo-Duggan *et al.*, 2015) and 50 µL of ultrapure water were added to the tube, and gently mixed. The tube was incubated at 95°C-100°C for 10 min. Finally, beads were magnetically separated, and initial input (total protein), unbound fraction, wash, and IP eluate were stored at -20°C for up to three months and used for western blot analysis. Gel electrophoresis and western blot using anti-PpCESA3, anti-PpCESA5, anti-PpCESA6/7, and anti-PpCESA8 antibodies was carried out as described previously (Scavuzzo-Duggan *et al.*, 2015).

Sample Preparation for Mass Spectrometry

Immunoprecipitated samples for mass spectrometry were processed as described above but were eluted in 200 µL of elution buffer (8 M Urea,150 mM NaCl, 25 mM NH_4HCO_3), and the resulting samples were reduced for 30 min at 37°C with 5 mM dithiothreitol (DTT), alkylated for 30 minutes at 25°C with 15 mM Iodoacetamide (IAA), and then the alkylation reaction was quenched with 5 mM of DTT for 15 minutes at 25°C. Samples were diluted with 25 mM NH_4HCO_3 to a final concentration of 1.5 M Urea and digested with 2 µg of Sequencing Grade Modified Trypsin (Promega, Madison, WI, USA) at 37°C for 16 hours. Tryptic peptides were purified using HyperSep C18 reverse-phase columns (Thermo Scientific, San Jose, CA, USA) according to the manufacturer's instructions. Samples were then evaporated to dryness using a centrivap concentrator (Labconco, Kansas City, MO, USA).

Dried samples were resuspended in 200 µL of 100 mM triethyl ammonium bicarbonate. Each Tandem Mass Tag (TMT) sixplex label reagent, (0.8 mg; Thermo Fisher Scientific) was resuspended in 41µL of 100% (v/v) acetonitrile. Each protein sample was then combined with its

respective TMT label reagent and incubated at 25°C for 16 hours. After incubation, reactions were quenched with 8 µL of 5% (w/v) hydroxylamine, combined in equal amounts in a new tube, and TMT-labeled peptides were purified on HyperSep C18 columns as described above. The combined sample was eluted from the C18 column, vacuum-dried, and resuspended in 20µL of 0.1% (v/v) formic acid for mass spectrometry analysis as described below.

Mass Spectrometry

TMT-labeled peptides were separated using an UltiMate 3000 RSLCnano system (Thermo Scientific) on a self-packed UChrom C18 column (100 µm x 35 cm). Separation of the TMT-labeled samples was achieved using a 180-minute gradient of solvent B from 2-27% [solvent A 0.1% (v/v) formic acid; solvent B acetonitrile, 0.1% (v/v) formic acid] at 50°C using a digital Pico View nanospray source (New Objectives, Woburn, MA, USA). The nanospray source was modified with a custom-built column heater and an ABIRD background suppressor (ESI Source Solutions, Woburn, MA). A laser P-2000 micropipette puller (Sutter Instrument Co, Novato, CA, USA) was used to pull the self-packed column tapered tip to an internal diameter of approximately 10 µm. The column was then sequentially packed with 1-2 cm of 5 µm Sepax GP-C18 (120A) (Sepax Technologies, Newark, DE, USA), and 40 cm of 1.8 µm Sepax GP-C18 (120A) at 9000 psi using a nano LC column packing kit (nanoLCMS, Gold River, CA, USA).

Mass spectrometry was performed on an Orbitrap Fusion mass spectrometer (Thermo Scientific). An MS^3 multi-notch approach was used for TMT analysis as previously described (McAlister et $al.$, 2014). The precursor selection range of the MS^1 is from 400-1400 m/z at a resolution of 120K, and an automatic gain control (AGC) target of 2.0 x 10^5 with a maximum injection time of 100 ms. Quadrupole isolation at 0.7 Th for MS^2 analysis was performed using CID fragmentation in the linear ion trap with a collision energy of 35%. The AGC was set to 4.0 x 10^3 with a maximum injection time of 150ms. A top speed data-dependent mode was used to operate the instrument with a most intense precursor priority. Dynamic exclusion was set to an exclusion duration of 60 s with a 10 ppm tolerance. The MS^3 precursor population was used to capture MS^2 fragment ions. The MS^3 precursors were then isolated within a window of 2.5 Da, and then a high energy collision induced dissociation was administered with a collision energy of 55%. The ions were detected at a resolution of 60,000 with an AGC of 5.0 x 10^4 and a maximum

injection time of 150ms within the Orbitrap. Data analysis was performed using Sequest (Thermo Scientific, v.27 rev.11) and Proteome Discover (Thermo Scientific, v.2.1).

The resulting mass spectrometry data was searched against the *Physcomitrella patens* UNIPROT database. Data was searched using SEQUEST with the following settings: 2 maximum missed tryptic cleavage sites, a precursor mass tolerance of 10 ppm, fragment mass tolerance of 0.6 Da. Methionine oxidation, phosphorylation, N-terminal acetylation, and cysteine carbidomethylation were included as dynamic modifications. TMT tags were included in the search parameters as static modifications. A decoy database was also searched to achieve a false discovery rate (FDR) of less than 0.5%. The full dataset containing all identified peptides in this experiment is included in supplemental data.

MbYTH assay

Interactions between PpCESAs were tested using an MbYTH assay according to the protocol provided by the kit manufacturer (DUAL membrane Kit 1, DualSystems Biotech AG). PpCESAs bait and prey vectors or control vectors provided in the kit were co-transformed into yeast strain NMY51. Co-transformants were cultured for 3 d at 30°C on solid synthetic medium lacking leucine (auxotrophic selection marker for the bait vector p TFB1) and tryptophan (auxotrophic selection marker for the prey vector pADSL-Nx). Expression of auxotrophic growth markers *ADE2* and *HIS3* was monitored by growth on medium lacking adenine and histidine in the presence of 3-aminotriazole (3-AT) (Timmers *et al.*, 2009). The two different auxotrophic markers and a colorimetric marker increased reliability. The bait was also screened in selection medium containing 3-AT to test for auto activation. To quantify the interactions for different preys, 100 colonies of each bait and prey combination were streaked on selective medium with 3-AT and counted after three days.

BiFC assay

The BiFC assay was used to analyze the interaction between the different PpCESAs *in planta*. Leaves of 3-week-old *N. benthamiana* plants were infiltrated with *Agrobacterium tumefaciens* strain GV3101pMP90 that had been transformed with various combinations of N-YFP-PpCESA and C-YFP-PpCESA test vectors and aquaporin N-YFP-PIP2-1 and C-YFP-PIP2-1 control vectors (Desprez *et al.*, 2007). YFP fluorescence was imaged three days after

infiltration using the 514-nm laser line of a SP2 AOBS Confocal Laser Scanning Microscope (CLSM, Leica, Solms, Germany) equipped with an argon laser. YFP reconstitution was tested by spectral analysis with the 496-nm laser line.

Accession numbers

Pp-CESA3, PNR49373.1; Pp-CESA6, AAZ86086.1; Pp-CESA7, AAZ86087.1; Pp-CESA8, ABI78961.1.

Conflicts of Interest

The authors declare that there are no conflicts of interest.

Data Availability

All data are reported within the paper and the supplemental files.

Legends for Supporting Information

Table S1. Primers used in this study.

Table S2. Peptide antigens, designed to regions of each PpCESA, used to raise specific antibodies for each PpCESA isoform.

Figure S1. RT-qPCR analysis of *PpCESA* expression in the KO mutants.

Figure S2. Quantitative analysis of S4B fluorescence intensity in leaf midribs of *P. patens* wild type, *ppcesa* knockout lines, and *ppcesa* knockout lines expressing cognate *HA-PpCESA*s.

Supplemental data. Peptide identifications for all proteins identified by Co-IP mass spectrometry.

References

Arioli, T., Peng, L., Betzner, A.S., Burn, J., Wittke, W., Herth, W., Camilleri, C., Höfte, H., Plazinski, J., Birch, R., Cork, A., Glover, J., Redmond, J. and Williamson, R.E. (1998) Molecular analysis of cellulose biosynthesis in *Arabidopsis*. *Science*, **279**, 717-720.

Atanassov, I.I., Pittman, J.K. and Turner, S.R. (2009) Elucidating the mechanisms of assembly and subunit interaction of the cellulose synthase complex of Arabidopsis secondary cell walls. *J Biol Chem*, **284**, 3833-3841.

Betancur, L., Singh, B., Rapp, R.A., Wendel, J.F., Marks, M.D., Roberts, A.W. and Haigler, C.H. (2011) Phylogenetically distinct cellulose synthase genes support secondary wall thickening in arabidopsis shoot trichomes and cotton fiber. *J Integr Plant Biol*, **52**, 205-220.

Brown, D.M., Zeef, L.A., Ellis, J., Goodacre, R. and Turner, S.R. (2005) Identification of novel genes in Arabidopsis involved in secondary cell wall formation using expression profiling and reverse genetics. *Plant Cell*, **17**, 2281-2295.

Burn, J.E., Hocart, C.H., Birch, R.J., Cork, A.C. and Williamson, R.E. (2002) Functional analysis of the cellulose synthase genes *CesA1*, *CesA2*, and *CesA3* in Arabidopsis. *Plant Physiol.*, **129**, 797-807.

Carroll, A., Mansoori, N., Li, S., Lei, L., Vernhettes, S., Visser, R.G., Somerville, C., Gu, Y. and Trindade, L.M. (2012) Complexes with mixed primary and secondary cellulose synthases are functional in Arabidopsis plants. *Plant Physiol*, **160**, 726-737.

Carroll, A. and Specht, C.D. (2011) Understanding plant cellulose synthases through a comprehensive investigation of the cellulose synthase family sequences. *Front Plant Sci*, **2**, 5.

Delmer, D.P. (1999) Cellulose biosynthesis: Exciting times for a difficult field of study. *Annu Rev Plant Physiol Plant Mol Biol*, **50**, 245-276.

Desprez, T., Juraniec, M., Crowell, E.F., Jouy, H., Pochylova, Z., Parcy, F., Hofte, H., Gonneau, M. and Vernhettes, S. (2007) Organization of cellulose synthase complexes involved in primary cell wall synthesis in *Arabidopsis thaliana*. *Proc Natl Acad Sci U S A*, **104**, 15572-15577.

Doolittle, W.F. (2012) Evolutionary biology: A ratchet for protein complexity. *Nature*, **481**, 270-271.

Endler, A. and Persson, S. (2011) Cellulose synthases and synthesis in Arabidopsis. *Mol Plant*, **4**, 199-211.

Fagard, M., Desnos, T., Desprez, T., Goubet, F., Refregier, G., Mouille, G., McCann, M., Rayon, C., Vernhettes, S. and Höfte, H. (2000) *PROCUSTE1* encodes a cellulose synthase required for normal cell elongation specifically in roots and dark-grown hypocotyls of Arabidopsis. *Plant Cell*, **12**, 2409-2423.

Fetchko, M. and Stagljar, I. (2004) Application of the split-ubiquitin membrane yeast two-hybrid system to investigate membrane protein interactions. *Methods*, **32**, 349-362.

Finnigan, G.C., Hanson-Smith, V., Stevens, T.H. and Thornton, J.W. (2012) Evolution of increased complexity in a molecular machine. *Nature*, **481**, 360-364.

Ghosh, I., Hamilton, A.D. and Regan, L. (2000) Antiparallel leucine zipper-directed protein reassembly: applications to the green fluorescent protein. *J Am Chem Soc*, **122**, 2658-5659.

Gonneau, M., Desprez, T., Guillot, A., Vernhettes, S. and Hofte, H. (2014) Catalytic subunit stoichiometry within the cellulose synthase complex. *Plant Physiol*, **166**, 1709-1712.

Goss, C.A., Brockmann, D.J., Bushoven, J.T. and Roberts, A.W. (2012) A *CELLULOSE SYNTHASE* (*CESA*) gene essential for gametophore morphogenesis in the moss *Physcomitrella patens*. *Planta*, **235**, 1355-1367.

Guerriero, G., Fugelstad, J. and Bulone, V. (2010) What do we really know about cellulose biosynthesis in higher plants? *J Integr Plant Biol*, **52**, 161-175.

Haigler, C.H. and Roberts, A.W. (2018) Structure/function relationships in the rosette cellulose synthesis complex illuminated by an evolutionary perspective. *Cellulose*.

Hamann, T., Osborne, E., Youngs, H.L., Misson, J., Nussaume, L. and Somerville, C. (2004) Global expression analysis of *CESA* and *CSL* genes in Arabidopsis. *Cellulose*, **11**, 279-286.

Hill, J.L., Jr., Hammudi, M.B. and Tien, M. (2014) The Arabidopsis cellulose synthase complex: a proposed hexamer of CESA trimers in an equimolar stoichiometry. *Plant Cell*, **26**, 4834-4842.

Hill, J.L., Jr., Hill, A.N., Roberts, A.W., Haigler, C.H. and Tien, M. (2018) Domain swaps of Arabidopsis secondary wall cellulose synthases to elucidate their class specificity. *Plant Direct*, **2**, e00061.

Horstman, A., Tonaco, I.A., Boutilier, K. and Immink, R.G. (2014) A cautionary note on the use of split-YFP/BiFC in plant protein-protein interaction studies. *Int J Mol Sci*, **15**, 9628-9643.

Hu, C.D., Chinenov, Y. and Kerppola, T.K. (2002) Visualization of interactions among bZIP and Rel family proteins in living cells using bimolecular fluorescence complementation. *Mol Cell*, **9**, 789-798.

Hu, H., Zhang, R., Feng, S., Wang, Y., Wang, Y., Fan, C., Li, Y., Liu, Z., Schneider, R., Xia, T., Ding, S.Y., Persson, S. and Peng, L. (2018) Three AtCesA6-like members enhance biomass production by distinctively promoting cell growth in Arabidopsis. *Plant Biotechnol J*, **16**, 976-988.

Jarvis, M.C. (2018) Structure of native cellulose microfibrils, the starting point for nanocellulose manufacture. *Phil Trans R Soc A*, **376**.

Jokipii-Lukkari, S., Sundell, D., Nilsson, O., Hvidsten, T.R., Street, N.R. and Tuominen, H. (2017) NorWood: a gene expression resource for evo-devo studies of conifer wood development. *New Phytol*, **216**, 482-494.

Kimura, S., Laosinchai, W., Itoh, T., Cui, X., Linder, C.R. and Brown, R.M., Jr. (1999) Immunogold labeling of rosette terminal cellulose-synthesizing complexes in the vascular plant *Vigna angularis*. *Plant Cell*, **11**, 2075-2085.

Kumar, M., Atanassov, I. and Turner, S. (2016) Functional analysis of cellulose synthase CESA protein class-specificity. *Plant Physiol*, **173**, 970-983.

Kumar, M., Thammannagowda, S., Bulone, V., Chiang, V., Han, K.H., Joshi, C.P., Mansfield, S.D., Mellerowicz, E., Sundberg, B., Teeri, T. and Ellis, B.E. (2009) An update on the nomenclature for the cellulose synthase genes in *Populus*. *Trends Plant Sci*, **14**, 248-254.

Lang, D., Ullrich, K.K., Murat, F., Fuchs, J., Jenkins, J., Haas, F.B., Piednoel, M., Gundlach, H., Van Bel, M., Meyberg, R., Vives, C., Morata, J., Symeonidi, A., Hiss, M., Muchero, W., Kamisugi, Y., Saleh, O., Blanc, G., Decker, E.L., van Gessel, N., Grimwood, J., Hayes, R.D., Graham, S.W., Gunter, L.E., McDaniel, S.F.,

Hoernstein, S.N.W., Larsson, A., Li, F.W., Perroud, P.F., Phillips, J., Ranjan, P., Rokshar, D.S., Rothfels, C.J., Schneider, L., Shu, S., Stevenson, D.W., Thummler, F., Tillich, M., Villarreal Aguilar, J.C., Widiez, T., Wong, G.K., Wymore, A., Zhang, Y., Zimmer, A.D., Quatrano, R.S., Mayer, K.F.X., Goodstein, D., Casacuberta, J.M., Vandepoele, K., Reski, R., Cuming, A.C., Tuskan, G.A., Maumus, F., Salse, J., Schmutz, J. and Rensing, S.A. (2018) The Physcomitrella patens chromosome-scale assembly reveals moss genome structure and evolution. *Plant J*, **93**, 515-533.

Le Bail, A., Scholz, S. and Kost, B. (2013) Evaluation of reference genes for RT qPCR analyses of structure-specific and hormone regulated gene expression in *Physcomitrella patens* gametophytes. *PLoS One*, **8**, e70998.

Li, S., Lei, L. and Gu, Y. (2013) Functional analysis of complexes with mixed primary and secondary cellulose synthases. *Plant Signal Behav*, **8**, e23179.

Li, X. (2017) Characterization of cellulose synthesis complexes and *Physcomitrella patens*. In *Cell and Molecular Biology*: University of Rhode Island.

Livak, K.J. and Schmittgen, T.D. (2001) Analysis of relative gene expression data using real-time quantitative PCR and the 2(-ΔΔC(T)) Method. *Methods*, **25**, 402-408.

Magliery, T.J., Wilson, C.G., Pan, W., Mishler, D., Ghosh, I., Hamilton, A.D. and Regan, L. (2005) Detecting protein-protein interactions with a green fluorescent protein fragment reassembly trap: scope and mechanism. *Journal of the American Chemical Society*, **127**, 146-157.

McAlister, G.C., Nusinow, D.P., Jedrychowski, M.P., Wuhr, M., Huttlin, E.L., Erickson, B.K., Rad, R., Haas, W. and Gygi, S.P. (2014) MultiNotch MS3 enables accurate, sensitive, and multiplexed detection of differential expression across cancer cell line proteomes. *Anal Chem*, **86**, 7150-7158.

McFarlane, H.E., Doring, A. and Persson, S. (2014) The cell biology of cellulose synthesis. *Annu Rev Plant Biol*, **65**, 69-94.

Nixon, B.T., Mansouri, K., Singh, A., Du, J., Davis, J.K., Lee, J.G., Slabaugh, E., Vandavasi, V.G., O'Neill, H., Roberts, E.M., Roberts, A.W., Yingling, Y.G. and Haigler, C.H. (2016) Comparative structural and computational analysis supports eighteen cellulose synthases in the plant cellulose synthesis complex. *Sci Rep*, **6**, 28696.

Norris, J.H., Li, X., Huang, S., Van de Meene, A.M.L., Tran, M.L., Killeavy, E., Chaves, A.M., Mallon, B., Mercure, D., Tan, H.-T., Burton, R.A., Doblin, M.S., Kim, S.H. and Roberts, A.W. (2017) Functional specialization of cellulose synthase isoforms in a moss shows parallels with seed plants. *Plant Physiol*, **175**, 210-222.

Persson, S., Paredez, A., Carroll, A., Palsdottir, H., Doblin, M., Poindexter, P., Khitrov, N., Auer, M. and Somerville, C.R. (2007) Genetic evidence for three unique components in primary cell-wall cellulose synthase complexes in Arabidopsis. *Proc Natl Acad Sci U S A*, **104**, 15566-15571.

Persson, S., Wei, H., Milne, J., Page, G.P. and Somerville, C.R. (2005) Identification of genes required for cellulose synthesis by regression analysis of public microarray data sets. *Proc Natl Acad Sci U S A*, **102**, 8633-8638.

Purushotham, P., Cho, S.H., Díaz-Moreno, S.M., Kumar, M., Nixon, B.T., Bulone, V. and Zimmer, J. (2016) A single heterologously expressed plant cellulose synthase isoform is sufficient for cellulose microfibril formation in vitro. *Proc Natl Acad Sci U S A*, **113**, 11360–11365.

Robert, S., Mouille, G. and Höfte, H. (2004) The mechanism and regulation of cellulose synthesis in primary walls: lessons from cellulose-deficient Arabidopsis mutants. *Cellulose*, **11**, 351-364.

Roberts, A.W. and Bushoven, J.T. (2007) The cellulose synthase (*CESA*) gene superfamily of the moss *Physcomitrella patens*. *Plant Mol Biol*, **63**, 207-219.

Roberts, A.W., Dimos, C., Budziszek, M.J., Goss, C.A. and Lai, V. (2011) Knocking out the wall: protocols for gene targeting in *Physcomitrella patens*. *Meth Molec Biol*, **715**, 273-290.

Roberts, A.W., Roberts, E.M. and Haigler, C.H. (2012) Moss cell walls: structure and biosynthesis. *Front Plant Sci*, **3**, 166.

Scavuzzo-Duggan, T.R., Chaves, A.M. and Roberts, A.W. (2015) A complementation assay for in vivo protein structure/function analysis in *Physcomitrella patens* (Funariaceae). *App Plant Sci*, **3**, 1500023.

Scavuzzo-Duggan, T.R., Chaves, A.M., Singh, A., Sethaphong, L., Slabaugh, E., Yingling, Y.G., Haigler, C.H. and Roberts, A.W. (2018) Cellulose synthase 'class specific regions' are intrinsically disordered and functionally undifferentiated. *J Integr Plant Biol*, **60**, 481-497.

Scheible, W.-R., Eshed, R., Richmond, T., Delmer, D. and Somerville, C. (2001) Modifications of cellulose synthase confer resistance to isoxaben and thiazolidinone herbicides in *Arabidopsis Ixr1* mutants. *Proc Natl Acad Sci USA*, **98**, 10079-10084.

Sethaphong, L., Haigler, C.H., Kubicki, J.D., Zimmer, J., Bonetta, D., DeBolt, S. and Yingling, Y.G. (2013) Tertiary model of a plant cellulose synthase. *Proc Natl Acad Sci U S A*, **110**, 7512-7517.

Somerville, C. (2006) Cellulose synthesis in higher plants. *Annu Rev Cell Dev Biol*, **22**, 53-78.

Song, D., Shen, J. and Li, L. (2010) Characterization of cellulose synthase complexes in Populus xylem differentiation. *New Phytol*, **187**, 777-790.

Taylor, N.G. (2008) Cellulose biosynthesis and deposition in higher plants. *New Phytol*, **178**, 239-252.

Taylor, N.G., Howells, R.M., Huttly, A.K., Vickers, K. and Turner, S.R. (2003) Interactions among three distinct CesA proteins essential for cellulose synthesis. *Proc Natl Acad Sci U S A*, **100**, 1450-1455.

Taylor, N.G., Laurie, S. and Turner, S.R. (2000) Multiple cellulose synthase catalytic subunits are required for cellulose synthesis in Arabidopsis. *Plant Cell*, **12**, 2529-2539.

Taylor, N.G., Scheible, W.-R., Cutler, S., Somerville, C.R. and Turner, S.R. (1999) The *irregular xylem3* locus of Arabidopsis encodes a cellulose synthase required for secondary cell wall synthesis. *Plant Cell*, **11**, 769-779.

Timmers, J., Vernhettes, S., Desprez, T., Vincken, J.P., Visser, R.G. and Trindade, L.M. (2009) Interactions between membrane-bound cellulose synthases involved in the synthesis of the secondary cell wall. *FEBS Lett.*, **583**, 978-982.

Tran, M.L., McCarthy, T.W., Sun, H., Wu, S.-Z., Norris, J.H., Bezanilla, M., Vidali, L., Anderson, C.T. and Roberts, A.W. (2018) Direct observation of the effects of cellulose synthesis inhibitors using live cell imaging of Cellulose Synthase (CESA) in *Physcomitrella patens*. *Sci Rep*, **8**, 735.

Tran, M.L. and Roberts, A.W. (2016) *Cellulose synthase* (*CESA*) gene expression profiling of *Physcomitrella patens*. *Plant Biol*, **18**, 362–368.

Turner, S. and Kumar, M. (2018) Cellulose synthase complex organization and cellulose microfibril structure. *Phil Trans R Soc A*, **376**.

Turner, S.R. and Somerville, C.R. (1997) Collapsed xylem phenotype of Arabidopsis identifies mutants deficient in cellulose deposition in the secondary cell wall. *Plant Cell*, **9**, 689-701.

Turner, S.R., Taylor, N. and Jones, L. (2001) Mutations of the secondary cell wall. *Plant Mol Biol*, **47**, 209-219.

Vidali, L., Burkart, G.M., Augustine, R.C., Kerdavid, E., Tuzel, E. and Bezanilla, M. (2010) Myosin XI is essential for tip growth in Physcomitrella patens. *Plant Cell*, **22**, 1868-1882.

Walter, M., Chaban, C., Schutze, K., Batistic, O., Weckermann, K., Nake, C., Blazevic, D., Grefen, C., Schumacher, K., Oecking, C., Harter, K. and Kudla, J. (2004) Visualization of protein interactions in living plant cells using bimolecular fluorescence complementation. *Plant J*, **40**, 428-438.

Wise, H.Z., Saxena, I.M. and Brown, R.M., Jr. (2011) Isolation and characterization of the cellulose synthase genes *PpCesA6* and *PpCesA7* in *Physcomitrella patens*. *Cellulose*, **18**, 371-384.

Yin, Y., Huang, J. and Xu, Y. (2009) The cellulose synthase superfamily in fully sequenced plants and algae. *BMC Plant Biol*, **9**, 99.

Zeng, L., Zhang, Q., Sun, R., Kong, H., Zhang, N. and Ma, H. (2014) Resolution of deep angiosperm phylogeny using conserved nuclear genes and estimates of early divergence times. *Nat commun*, **5**, 4956.

Table 1. Enriched proteins co-immunoprecipitating with PpCESA3.

Uniprot ID[a]	Uniprot Annotation[b]	Abundance ratio[c] (HA-CESA3/ control)	Abundance Ratio Adj. P-value[d]	% coverage[e]	# of peptides identified[f]	Unique peptides[g]	Sub-cellular localization[h]
A9RGN5	Cellulose synthase 3	10.949	6.4×10^{-3}	24	21	8	PM
Q6YXQ2	Photosystem I iron-sulfur center	7.868	4.5×10^{-2}	73	5	5	Chloro
Q06FC6	Cellulose synthase 8	7.793	1.7×10^{-2}	16	15	1	PM
A9S9W2	Uncharacterized protein	7.519	1.3×10^{-2}	2	1	1	PM
A9RLI3	Golgi SNAP receptor complex member 1	7.491	1.7×10^{-2}	4	1	1	GA
A9RFD0	Transmembrane 9 superfamily member	6.669	6.2×10^{-2}	1	1	1	PM
A9RKD2	Predicted protein	6.427	7.9×10^{-2}	7	1	1	V; M
Q06FC7	Cellulose synthase 7	6.214	2.0×10^{-2}	10	10	3	PM
Q6YXK2	ATP synthase subunit b	6.166	2.3×10^{-2}	5	1	1	Chloro
A7IZE8	PHO1-3	5.758	6.0×10^{-2}	1	1	1	PM
A9SSB6	Cytochrome b6-f complex iron-sulfur subunit	5.75	4.1×10^{-2}	7	1	1	PM
A9TU19	Predicted protein	5.439	6.5×10^{-4}	9	2	2	Me
A9RS00	Predicted protein	5.339	5.5×10^{-2}	2	1	1	PM
A9TTQ2	Predicted protein	5.094	1.8×10^{-2}	13	3	1	M
A9TJ92	Cellulose synthase-like D1	5.015	1.1×10^{-2}	4	4	4	GA
A9U226	Chlorophyll a-b binding protein	4.859	1.7×10^{-2}	7	2	1	Chloro
A9REG3	Predicted protein	4.767	2.0×10^{-2}	45	9	3	Chloro
A9RJU8	Predicted protein	4.665	1.2×10^{-2}	16	3	3	NP
A9RPU6	Predicted protein	4.509	1.1×10^{-2}	5	1	1	Chloro
A9SYK6	Predicted protein	4.454	1.7×10^{-2}	7	4	4	PM
A9SHP6	Predicted protein	4.438	2.6×10^{-2}	10	2	1	PM; Chloro
A9TFG8	R-SNARE, VAMP72-family	4.347	2.7×10^{-2}	21	4	1	PM; SC
A9T399	Chlorophyll a-b binding protein	4.165	7.2×10^{-3}	14	4	1	Chloro

[a] Uniprot Protein ID (http://www.uniprot.org/)
[b] Uniprot Protein Annotation (http://www.uniprot.org/)
[c] Abundance ratios of peptides identified in HA-PpCESA3 IP relative to control (Supplemental data)
[d] P-value adjusted using Benjamin-Hochberg correction for false-discovery rate (Supplemental data)
[e] Percent peptide coverage of each identified protein
[f] Total number of peptides identified for each protein
[g] Number of peptides uniquely mapped to the identified protein
[h] Uniprot annotation of sub-cellular localization (http://www.uniprot.org/)

Abbreviations: PM – Plasma Membrane; C- Chloroplast; GA – Golgi Apparatus; V – Vacuole; M – Mitochondria; Me – Membrane; SC – SNARE complex; NP – Not Predicted

Table 2: Summary of results from membrane-based yeast two-hybrid (MbYTH)/bimolecular fluorescence complementation (BiFC) protein interaction assays.

Weak interaction (W) for MbYTH were more than twice the negative controls, but less than half of the positive control.

BAIT/N-YFP	PpCESA3	PpCESA8	PpCESA6	PpCESA7
PpCESA3	W/-	-/W	-/-	W/+
PpCESA8	+/+	-/-	W/W	+/+
PpCESA6	-/-	+/+	-/-	+/+
PpCESA7	+/+	-/-	+/+	+/+

Figures

	PpCESA3	PpCESA5	PpCESA8	PpCESA4	PpCESA7	PpCESA10
*ppcesa3*KO	NA	0.94/1.34	1.59 +*	0.86/0.79	0.97/0.78	0.86/0.76
*ppcesa8*KO	0.80 /0.80	1.06/1.31	NA	0.97/0.98	0.86/1.45	0.81/1.02
*ppcesa3/8*KO	NA	1.77/1.78 +*	NA	0.65 /0.74	0.60/0.67 -*	0.99/1.01
*ppcesa4/10*KO	1.02/0.90	1.14/0.96	0.92/1.07	NA	1.25/1.13	NA
*ppcesa6/7*KO	0.48/0.58 -*	0.91/0.80	0.57/0.5 -*	0.73/0.72 -*	NA	0.92/0.67

Figure 1: RT-qPCR analysis *PpCESA* expression in *ppcesa*KO mutants. CESA expression relative to *PpACT* and *PpVHP* reference genes was determined for RNA isolated from gametophores harvested from 21-day old cultures of wild type (3 independent isolations) and *ppcesa*KOs (3 independent lines per genotype). Fold changes in gene expression compared to wild type ($2^{-\Delta\Delta Ct}$, n=3) are reported for two independent RNA isolations separated by /. Colors/* indicate results of non-parametric statistical analysis comparing $2^{-\Delta Ct}$ values for *ppcesa*KO genotypes to wild type for the combined results of two independent RNA isolations (n=6): blue/-*=significant down-regulation, $p<0.05$; gray=no significant difference, $p>0.05$; orange/+*=significant up-regulation, $p<0.05$; white=no measurable expression). Results are shown graphically in **Supplemental Figure 1.**
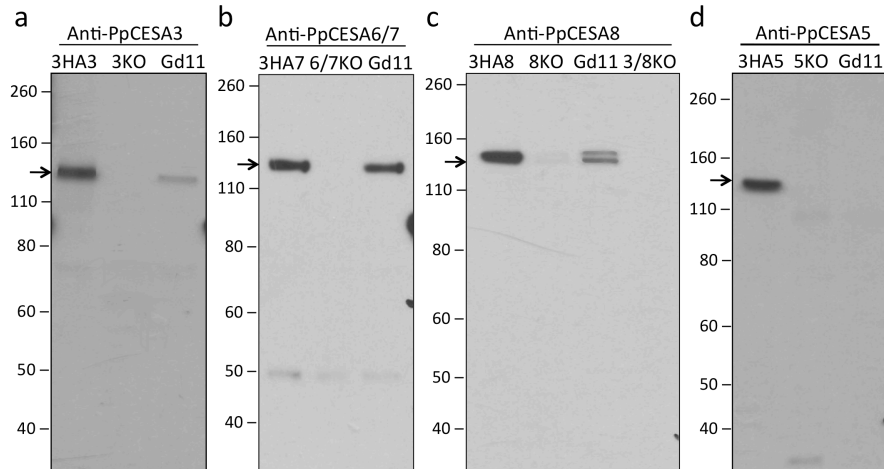
Figure 2: Antibody specificity test. Western blots of microsomal protein extracts from HA-tagged PpCESA overexpression lines (positive control), PpCESA knock out (KO) lines (negative control), and wild-type probed with **(a)** anti-PpCESA3, **(b)** anti-PpCESA6/7, **(c)** anti-PpCESA8, and **(d)** anti-PpCESA5. Molecular mass markers are given at left in kilodaltons. Black arrows indicate expected position of target bands (~120 kDa) detected by antibodies. Faint band in 8KO lane, but not 3/8KO line in **c**, indicates weak cross reactivity of anti-PpCESA8 with PpCESA3.
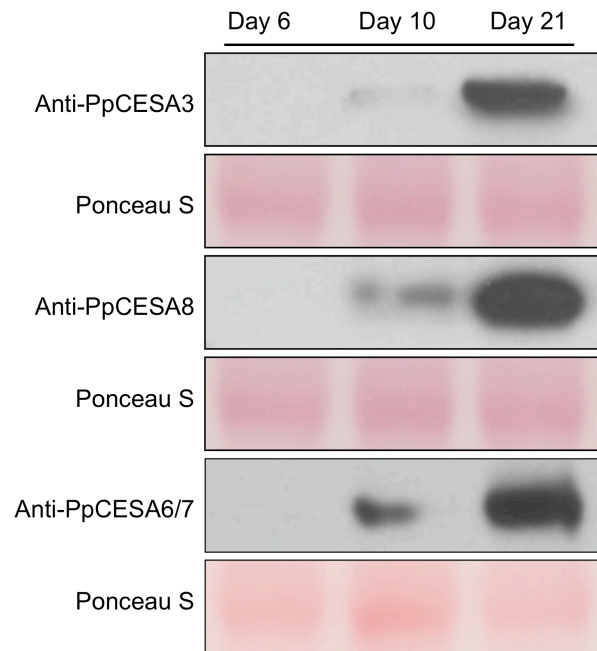
Figure 3: PpCESA protein expression in wild-type *P. patens*. Western blots of microsomal proteins isolated from wild-type *P. patens* cultures and probed with anti-PpCESA3, anti-PpCESA8, and anti-PpCESA6/7. Explants from protonema cultured on solid medium overlaid with cellophane for 6 days were cultured on solid medium without cellophane and harvested after 6 days (protonema only), 10 days (protonema and young gametophores) and 21 days (gametophores). Equal loading of protein (9.6 μg per lane) was verified by Ponceau S Staining.
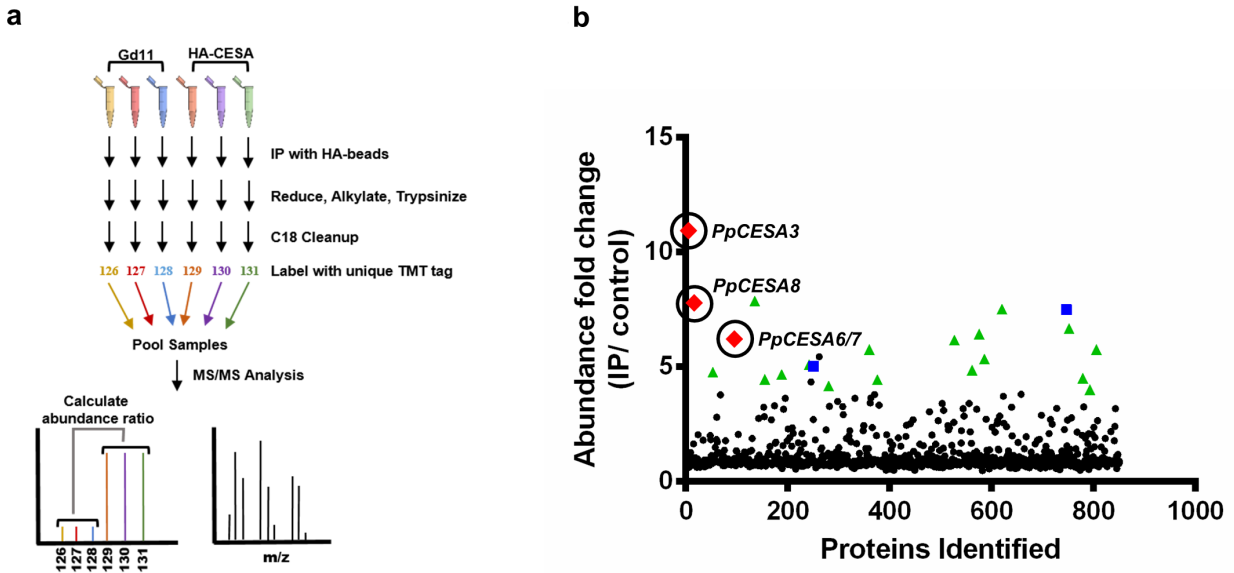
Figure 4. Quantitative proteomics analysis of PpCESA immunoprecipitated samples. (a) A representative workflow schematic of PpCESA IP sample processing is shown. Solubilized membrane extracts from three independent non-transgenic Gd11 samples or the respective HA-PpCESA transgenic line were prepared and subjected to anti-HA affinity chromatography. Each sample was independently prepared for mass spectrometry and labeled with a unique TMT isobaric tag. The labeled samples were pooled and subjected to mass spectrometry. TMT isobaric tag signals for each identified peptide were used to quantify abundance ratios of proteins that were over-represented in anti-HA enriched samples compared to wild-type Gd11 controls. **(b)** The IP/ control abundance ratios for all proteins identified in PpCESA3 IP experiments are shown. Immunoprecipitated CESA proteins are shown in red (diamonds), abundant photosynthetic proteins are shown in green (triangles), and other abundant proteins are shown in blue (squares). Proteins that were not enriched greater than 4-fold are indicated as black points. Each point represents the average abundance fold change from all peptides originating from a particular protein.
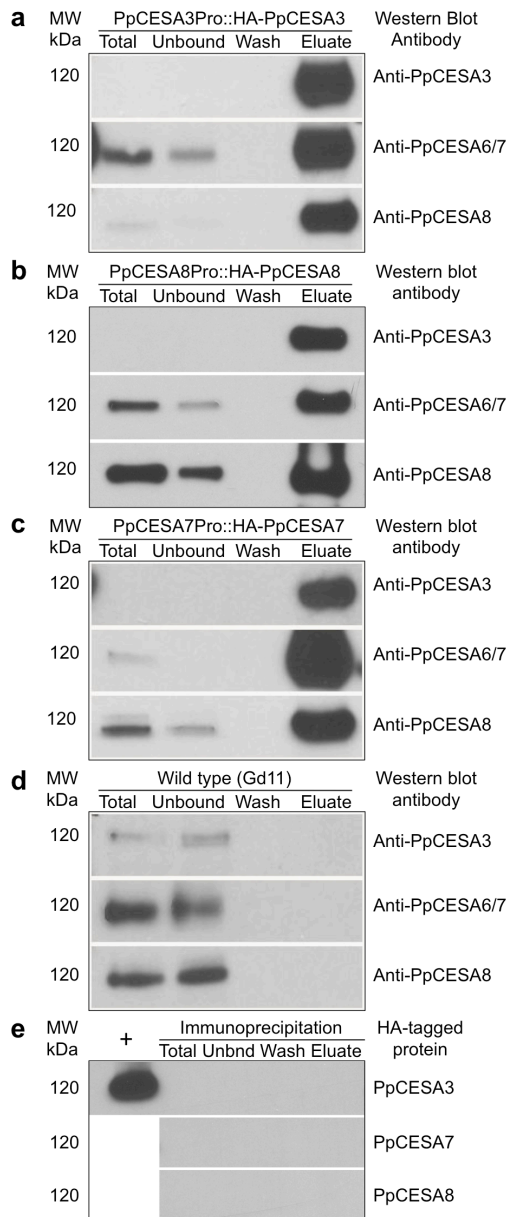
Figure 5: Co-immunoprecipitation (Co-IP) of PpCESAs. Western blots of total protein lysates from the indicated transgenic lines expressing HA-PpCESAs under control of their native promoters (**a-c**) and GD11 wild type (**d**) with unbound, wash and eluate from immunoprecipitation with anti-HA. Blots were probed with antibodies listed on the right of each panel. (**e**) Twelve IP fractions from **a-c** above, probed with Anti-CESA5. Positive control HA-CESA5 (+) was included because PpCESA5 is not detectable in total proteins extracts from wild-type gametophores. All 12 extracts and the positive control were run and probed together.
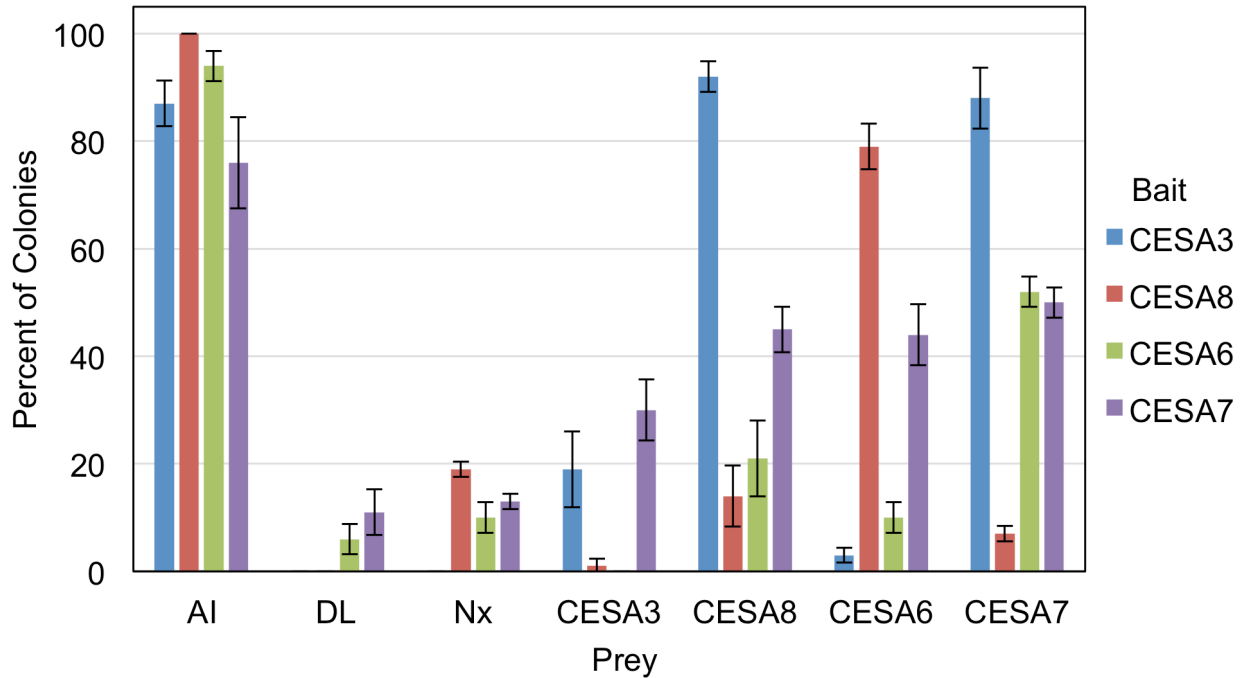
Figure 6. Interactions between PpCESAs measured by MbYTH assay. Yeast expressing each of the PpCESAs as bait with the ALG5 protein fused to NubI as positive control (AI) and NubG as negative control (DL) and an empty prey vector as another negative control (Nx) and the same PpCESA proteins fused to NubG, as prey were tested. The percentage of colonies that show visible growth after 5 days at 30°C on selective medium is shown with errors bars representing standard deviation (n=3).
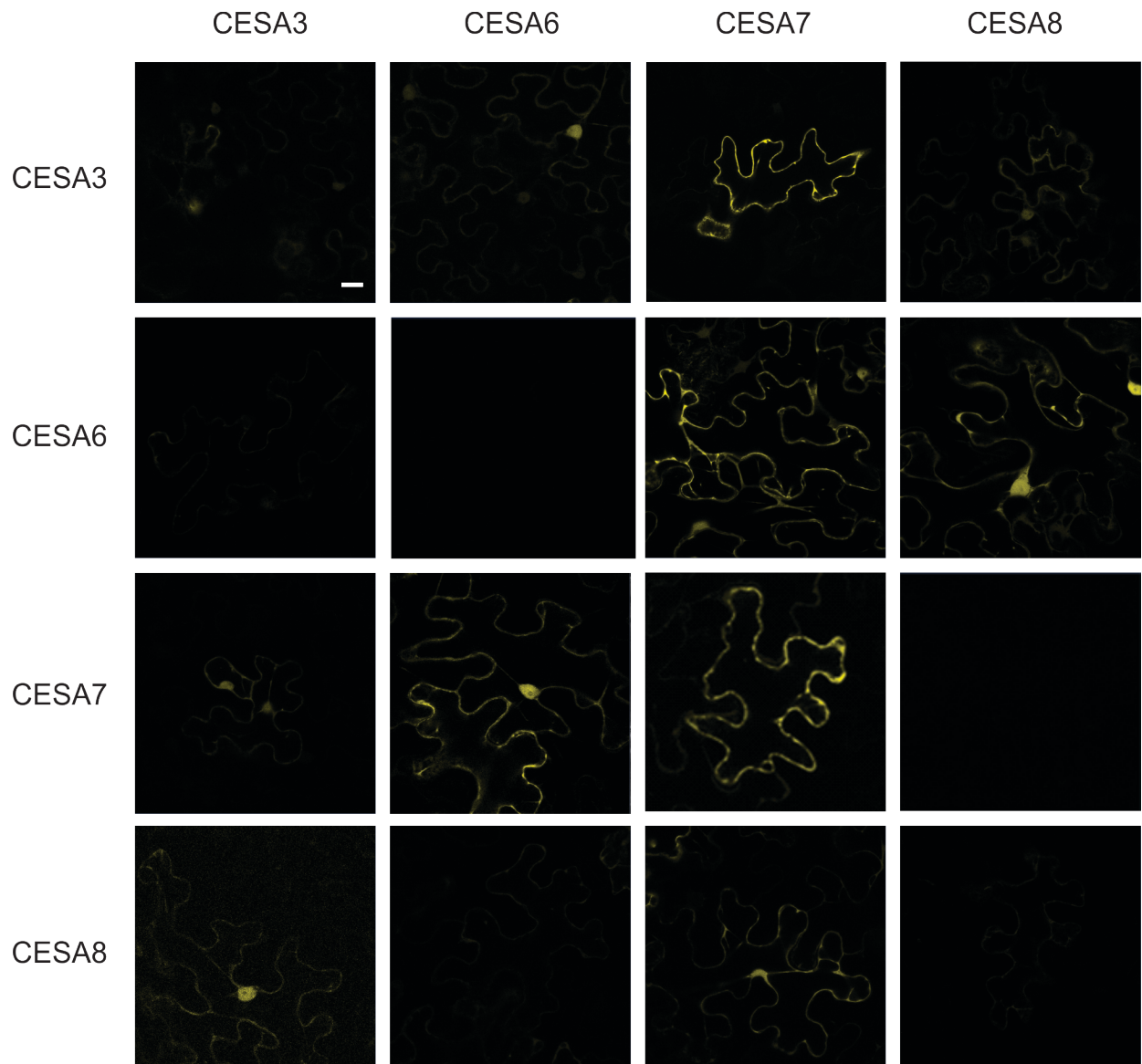
Figure 7. *In vivo* **dimerization of PpCESAs measured by BiFC in** *N. benthamiana* **leaf epidermal cells**. Confocal images of epidermal cells co-transformed with C-YFP-PpCESAs (top) and N-YFP-CESAs (left). Scale bar = 20µm. Magnification is identical for all images.
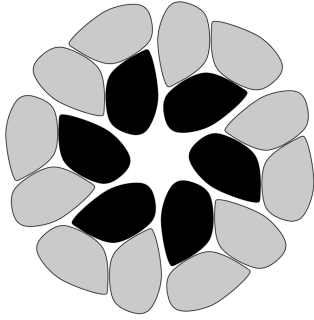
Figure 8: Conceptual model of a secondary cell wall CSC from *P. patens*. Gray and black represent class A (PpCESA3 or PpCESA8) vs. class B (PpCESA6 or PpCESA7) subunits. See text for further explanation.